New insights into the recent eruptive history of Montagne Pelée (Lesser Antilles Arc) from offshore marine drilling site U1401A (IODP Expedition 340)

Clara Solaro, Georges Boudon, Anne Le Friant, Hélène Balcone-Boissard, Laurent Emmanuel, Martine Paterne

New insights into the recent eruptive history of Montagne Pelée (Lesser Antilles arc) from offshore marine drilling site U1401A (340 Expedition IODP)

Clara Solaro [a], Georges Boudon [a], Anne Le Friant [a], Hélène Balcone-Boissard [b], Laurent Emmanuel [b], Martine Paterne [c], and IODP Expedition Science Party

[a] *Université de Paris, Institut de physique du globe de Paris, CNRS, F-75005 Paris, France.*

[b] *Sorbonne Université, Institut des Sciences de la Terre de Paris (ISTeP), UMR 7193, 4 place Jussieu, 75005 Paris, France.*

[c] *LSCE, - UMR 8212 - CEA-CNRS UVSQ/IPSL, Avenue de la Terrasse, Domaine du CNRS, 91198 Gif Sur Yvette Cedex - France*

Key words : Montagne Pelée, Tephrochronology, eruptive history, flank-collapse, IODP expedition 340

Corresponding author: **Georges Boudon** (boudon@ipgp.fr)

Université de Paris, Institut de physique du globe de Paris, CNRS, F-75005 Paris, France.

Tel: 00 33 1 83 95 76 32

ABSTRACT

Marine tephrochronology provides a good alternative to study in depth the eruptive history of volcanic islands in a tropical climate and overcome the problem of poorly preserved outcropping. Here, we provide new observations on the recent volcanological evolution (< 40 kyrs) of Montagne Pelée (Martinique Lesser Antilles) based on the tephrochonological study of a marine core from the site U1401, sampled during the 340 IODP expedition and located 28 km from the coastline, west off Martinique Island. The core (15 m recovered length) was obtained from the debris avalanche deposits (DAD) due to the last flank collapse that occurred on Montagne Pelée volcano. Although it was not possible to drill through the DAD because of the heterogeneity of the deposit and the presence of large blocks, the sediments and volcanic deposits that covered the DAD were sampled. A detailed multiparameter study (geophysical data acquired on-board during the IODP cruise, lithological and geochemical data and temporal constrains through ^{18}O stratigraphy and ^{14}C dating) of the core U1401A suggest a new age for the last flank collapse leading us to update the volcanological recent history of Montagne Pelée. The last flank collapse is now dated at ~36 cal. ka BP (older than previous studies). The flank collapse, even though it wasn't voluminous (2 km^3), had a significant consequence on the magma plumbing system of Montagne Pelée and produced, by the threshold effect exerted on the plumbing system, abundant explosive eruptions with basaltic-andesite magmas, during the period 36-25 cal. ka BP. This new age obtained for this flank collapse has important implications not only for the post collapse activity, but also allows us to rethink the recent volcanological history of Montagne Pelée.

1. Introduction

The reconstruction of the eruptive history of a volcano relies mainly on historical chronicles and on geological studies of volcanic deposits in order to establish the most comprehensive stratigraphy. Geological studies face many problems, the first of which being the adequate preservation of key outcrops. This issue is of prime importance particularly in tropical environment where high precipitation rates and alteration processes destroy large proportions of volcanic deposits and abundant vegetation impairs on-land observations. Considering all these parameters and the recovery from eruptive products, it is difficult to achieve a detailed stratigraphy that stretches beyond a few thousand years. In a volcanic island context, to overcome this problem and go into further detail, marine tephrochronology provides a good alternative to complete the volcanological history for earlier periods. Reconstruction of volcanic activity and history have already been carried out on several volcanoes, using both marine or lacustrine tephrochronological data and on-land stratigraphy (Sigurdsson and Carey, 1981; Paterne et al., 1988; 1990, 2008; Wulf et al., 2004; Shane, 2000; Shane et al., 2006; Le Friant et al., 2008; Allan et al., 2008; Engwell et al, 2014; Jennings et a., 2014; Lowe, 2014; Weller et al., 2015).

In recent decades several cruises (Aguadomar-1999, Caraval-2002, JCR-2005, Gwadaseis-2009) have taken place off the Lesser Antilles islands. Geophysical data were acquired, and several piston cores were also sampled. The first meters of sediments have been documented and thus completing part of the volcanological history of some volcanoes such as Soufrière Hills volcano (Trofimovs et al. 2006; Le Friant et al., 2008; Wall-Palmer et al., 2012) or Montagne Pelée (Boudon et al., 2013). Deep drilling projects provide a unique opportunity to investigate sediments found several hundred meters deep and the volcanoclastic deposits from the surrounding volcanoes, sometimes going back several million years (Kutterolf et al., 2018). The 340 IODP Expedition (March-April 2012) aboard the *Joides Resolution*, drilled a series of sites offshore Montserrat, Martinique and Dominica

(Fig. 1a). The objectives of the project were 1/ to characterize the voluminous chaotic units identified off the islands associated with the volcanic island landslides (Brunet et al., 2016; Le Friant et al., 2015); 2/ to obtain a complete volcanological history of the surrounding volcanoes and to include the large mass wasting events in the evolution of the volcanoes (Wall-Palmer et al., 2014; Cassidy et al., 2015; Coussens et al., 2016)

The aim of this paper is to provide new insights on the last tens of thousands of years of Montagne Pelée's evolution based on the tephrochonological study of site U1401, sampled during the 340 IODP expedition and located west off Martinique Island, 28 km from the coastline (Fig.1b). By drilling through the DAD the objectives were to characterize and date the setting of the debris avalanche with associated erosional processes. Although it was not possible to drill through the DAD because of the heterogeneity of the deposit and the presence of large blocks (Le Friant et al., 2015), the pelagic sediments and volcanic deposits that covered the DAD were successfully sampled. They thus offer a good opportunity to study the post DAD volcanoclastic sedimentation processes and to better constrain the volcano's recent evolution.

2. Geological setting

Martinique Island is located in the southern part of the Lesser Antilles arc that result from the subduction of the northern and southern Atlantic plates beneath the Caribbean plate with a relatively slow rate of 2 cm/yr (Wadge, 1984). This southern part of the arc is bordered to the west by the 3000 m deep back-arc Grenada Basin (Fig. 1a). Montagne Pelée, the sole active volcano of Martinique island and one of the twelve active volcanoes of the arc, is located in

100 the northern part of Martinique, north of the old Morne Jacob – Pitons du Carbet volcano,
101 (Fig. 1b). It is a famous and tragic volcano as during the first months of the 1902-1905 dome-
102 forming eruption the towns of St. Pierre and Morne Rouge were destroyed by a series of
103 laterally directed explosions killing 30 000 inhabitants (Lacroix, 1904). The last eruptive
104 activity was the 1929-1932 lava dome-forming eruption (Perret, 1937).
105
106 *Previous works:* In the last decades and especially after the 1902-1905 eruption a lot of
107 studies were carried out on Montagne Pelée. Exclusively terrestrial studies were performed
108 until 1998 (Roobol and Smith, 1976; Westercamp and Traineau, 1983a, b; Bourdier et al.,
109 1985, 1989; Boudon and Lajoie, 1989; Boudon, 1993) whereas, after this date, combined on-
110 land and marine data were obtained through several cruises, field work and laboratory studies
111 (Deplus et al., 2001; Le Friant et al., 2003, 2015; Boudon et al., 2005, 2007, 2013; Brunet et
112 al., 2016).
113 Based on previous works, the volcanological evolution of Montagne Pelée was divided in
114 three eruptive phases. The first two phases ended in a large flank collapse. (Fig.1c, Le Friant
115 et al., 2003; Boudon et al., 2005, 2007, 2013; Brunet et al., 2016).
116 The first eruptive phase resulted in a first volcanic edifice that was destroyed by a large flank
117 collapse (Le Prêcheur event) that produced a 8 x 6 km large horseshoe-shaped structure
118 (without the invisible southern rim) and a debris avalanche of ~25 km^3 that flowed into the
119 Grenada basin (Le Friant et al., 2003; Boudon et al., 2007). Using K-Ar ages acquired from
120 lava domes and lava flows on the northern volcanic edifices of Montagne Pelée and Mont
121 Conil this event was dated at ~127 ka (Germa et al., 2011a).
122 The second eruptive stage created a new volcanic edifice inside and on the southern rim
123 of the first flank-collapse structure. Dome-forming eruptions and associated block- and ash
124 pyroclastic density currents involving acid magmas were the dominant activity of this period.

125 This volcanic edifice was destroyed by a second flank collapse (St Pierre event), which
126 generated a horseshoe-shaped structure, 6 x 4 km in size, and a debris avalanche (~13 km^3)
127 that flowed like the first one into the Grenada basin. By correlating stratigraphy and
128 magmatology of on-land deposits with tephra layers identified in a piston core (CAR-MAR 4)
129 drilled during the Caraval cruise northwest of Martinique (Fig. 1a), Boudon et al. (2013)
130 proposed a minimum age of 32 ka cal BP for this flank collapse.

131 The third eruptive stage, just after this flank collapse, generated more basic magmas
132 (basaltic andesite), with a high production rate, over several thousand years. After a decrease
133 in the magma production, activity resumed and the magma emitted, after and up to the
134 historic activity of Montagne Pelée, were again as acid as during the second eruptive stage.
135 Plinian to subplinian events and dome-forming eruptions were the two main eruptive styles
136 that occurred during this period. On-land studies recognized 10 plinian to subplinian events
137 and 18 dome-forming eruptions, including the two last historic eruptions, during the last 15
138 000 years of eruptive activity (Roobol and Smith, 1976; Westercamp and Traineau, 1983a, b;
139 Traineau et al., 1989; Smith and Roobol, 1990; Michaud-Dubuy, 2019). But
140 tephrochronological studies of the CAR-MAR 4 piston core showed that the number of
141 volcanic events identified on-land was underestimated particularly for the period prior to
142 5 000 years BP (Boudon et al., 2013).

143 During this third stage, a new flank-collapse occurred on the southwestern flank of the
144 volcano (Rivière Sèche event). Lower in volume than the previous ones (~2 km^3), the debris
145 avalanche flowed and stopped at the base of the submarine flank and exhibits a typical
146 hummocky morphology. U-Th dating on lava dome located inside the structure gives an age
147 of ~9 ka for this event (Le Friant et al., 2003).

148 On the basis on IODP core analysis, Le Friant et al. (2015) and Brunet et al. (2016) stated
149 that for the first flank collapse affecting Montagne Pelée volcano the debris avalanche entered

150 the sea, flowed over the submarine volcano slope, to stop and deposit around the slope break.
151 This first - and the largest - debris avalanche deposit loaded, weakened seafloor sediment.
152 Resulting submarine landslide propagates along a decollement surface, deforming in situ
153 alternation of hemipelagic sediments and turbidity deposits (Fig 1b). The debris avalanche
154 deposit generated by the second flank collapse may have locally remobilized sediments within
155 the submarine landslide deposit, by exerting normal stress that triggered the deformation
156 process.
157
158
159 **3. Materials and analytical methods**
160
161 *4.1. Coring and on-board observations*
162
163 The site U1401 consists of four different holes drilled along a transect 900 m long, NW-
164 SE direction, above the debris avalanche deposits (DAD) associated with the last flank
165 collapse generated by Montagne Pelée volcano (Fig. 1b). The hole U1401A, (14°39.10′N,
166 61°25.08′W; 2590 mbsl), is the longest of the four drilled holes at 15.61 m recovered length,
167 and has been chosen for this study. For each hole (example: U1401A), several 9 m long cores
168 were collected (example U1401A- 1H) and were cut in sections with a maximum length of
169 1.5 m (example: U1401A - 1H1). Each section was sawn lengthwise. One half was stored as
170 an archive (GCR – USIO, Texas A & M University College Station, Gulf Coast Repository)
171 and the other half was used for physical properties (magnetic susceptibility, gamma-ray
172 attenuation density, P-wave velocity), chemical analysis and lithological descriptions. On-
173 board each core was precisely described by sedimentologists and volcanologists in terms of
174 sedimentology, lithology and volcanic structures.

175

176 *4.2. Sampling*

177

178 For specific analysis, samples were taken according to their position in each section of
179 the core (example U1401A - 1H4, 93/95cm). A systematic sampling (every 10 cm) of the
180 hemipelagic sediments was carried outall along the core for $\delta^{18}O$ chronostratigraphy. For
181 lithological and chemical analyses of volcanic deposits, samples were taken from each deposit
182 that was visually identified within the core. In case of thick turbidity deposit, two or three
183 samples were taken, at the base, the middle and the top of the deposit, to observe potential
184 lithological variations.

185

186 *4.3. On board physical properties*

187

188 Magnetic susceptibility measurements were realized with the multisensor track (MST)
189 aboard the *Joides Resolution.* Closely spaced measurements (one point every 3cm) were
190 collected on the four cores of the site U1401. Magnetic susceptibility measurements provide
191 information on the content of magnetic minerals of each measured lithological level. Thus it
192 is possible to distinguish hemipelagic mud, characterized by a low amount of magnetic and
193 paramagnetic particles, from tephra layers and volcanic turbidity deposits, significantly
194 enriched with magnetic particles.

195 Gamma – ray attenuation density measurements were performed with the DSDP GRAPE
196 hardware and software. The system consists of a specific instrument that moves a section of
197 core in between a gamma-ray source and a detector. Measurements are based on the direct
198 correlation between the gamma-ray attenuation and the bulk density of the sample, which is

199 an indicator of lithological changes (minerals, grain size, porosity). The higher the bulk
200 density of the sample is, the higher is the attenuation.

201 Physical properties data need to be corrected due to data related to technical problems
202 occurring during measurements when moving from one section to another (i.e. aberrant
203 density values lower than 1 g/cm^3). For this reason, acquired measurements on a slice of 20
204 cm at the boundary between two successive sections were systematically removed.

205 We focused on magnetic susceptibility data as they exhibit more sensitive variations
206 along the core. Detailed information about lithological changes at a small scale (1 to 10 cm)
207 and identification of tephra layers within each section can be obtained using this dataset.

208

209 *3.4. ^{18}O stratigraphy*

210

211 To assess chronology of the volcanic deposits, hemipelagic sediment was sampled every
212 10 cm all along the core. However, the presence of thick turbidity deposits prevented us from
213 keeping a constant sampling interval all along the core. Turbidity deposits will be taken into
214 account in the interpretation of $\delta^{18}O$ curves. After being dried for about 12 hours at 70°C,
215 each sample was divided in two equal parts, one used for measurements and the other saved
216 as an archive. The former fraction was then weighed, sieved under water in a 40 µm stainless
217 steel sieve to remove fine particles, then dried again and finally weighed a second time. This
218 fraction was then divided in two halves, one for $\delta^{18}O$ chronostratigraphy and ^{14}C dating, the
219 second for lithological and mineralogical analysis.

220 For $\delta^{18}O$ chronostratigraphy, 3 to 4 planktotic foraminifera from the specific species of
221 *Globigerinoides ruber* (Alba White, D'Orbigny, 1839) were hand-picked in the fraction 250-
222 315 µm. Isotopic $\delta^{18}O$ analyses of foraminifera samples were performed at ISTeP (Sorbonne
223 Université), with a 3kV-Delta V Advantage IRMS attached to a Kiel IV Carbonate Device.

Isotope values are reported in conventional delta (δ) notation as per mil (‰) deviations of the isotopic ratios ($^{18}O/^{16}O$) calculated to the VPDB scale using an inhouse standard (Carrara Marble) calibrated against NBS-19. Standard deviation (1σ) for $\delta^{18}O$ measurements is 0.07 ‰.

4.5. ^{14}C dating

On the basis of the $\delta^{18}O$ curve, ^{14}C dates allow us to obtain absolute ages on key points of the curve to "calibrate" the timescale. For ^{14}C dating, 1000 planktonic foraminifera (about 14 mg required for spectrometer detection limit) were hand-picked in the fraction 250-315 µm of each sample. The ^{14}C analyses were performed at the French National AMS-ARTEMIS-LMC14 facility (Artemis Accelerator Mass Spectrometer, Saclay Laboratory, Université Paris-Saclay, France). The ^{14}C dating have been converted into calendar years using the Intcal 09 calibration record (Reimer et al., 2009; Hughen et al., 2004) taking into account the marine reservoir age correction of 400 years.

4.6. Lithological data

Lithologic analyses of turbidity deposits and tephra layers were performed on selected samples, chemically attacked with HCl (0.1 mol) to disaggregate all carbonate microfossils and carbonate non biogenic particles, rinsed with de-ionized water, dried and weighed. To remove all remnant fine particles, samples were then sieved in de-ionized water with a 40 µm stainless steel sieve, dried again for about 24 hours at 70°C, and weighed a second time. Each sample was divided in two equal parts, one fraction used for lithology and the other for geochemistry. Counting for lithology was done on 46 samples on the fraction > 125µm on a

basis of at least 400 particles/sample on a quadri plate under a binocular microscope. Five classes of clasts were identified: pumice and glass shard particles, scoria clasts, lava dome clasts, oxidized and hydrothermalized clasts and crystals (feldspars, orthopyroxenes, clinopyroxenes, amphiboles, oxides). The objective of counting is to identify the peak of abundance of the different volcanic clasts (scoria, pumice or lava domes clasts); They allow us to link the deposit to a specific eruptive style (pumices with plinian eruptions, scorias with explosive eruptions with more basic magma, and dense clasts with lava dome eruptions) and find some benchmark levels in the core. Counting precision has been estimated counting 6 times 6 different samples. The error linked to the operator is of about 10% based on the counting of the same sample by three different operators. The background signal was estimated counting about 400 clasts in some hemipelagic fractions of the core.

Moreover, detailed textures of volcanic clasts (vesicularity, microcristallinity) have been investigated using Back-Scattered Electron (BSE) images of pumice, scoria and lava dome clasts with a ZEISS-Supra 55 SEM (ISTeP, Sorbonne Université, Paris). Imaging was performed with an acceleration voltage of 15kV and a probe current of 5 nA.

4.7. Geochemical data: glass composition

Pumice and scoria clasts from each peak of abundance along the core were hand-picked in the sample fraction reserved for geochemistry, embedded in resin and polished. Major element composition of matrix glass was determined in 10 different tephra layers and 10 turbiditic levels using a CAMECA-SX 100 electron microprobe (Service Camparis, Paris, France). Analyses were performed with an acceleration voltage of 15 kV and a beam current of 4 nA. Counting time was of 5s on Na to limit Na migration, 10s for Si, Ti, Al, Fe, Mn,Mg,Ca, K, P and 15s for Cl. As recommended, we analyzed a minimum of 20 different

glass shards per level. However, depending on the level, between 5 and 30 glass shards were kept after detailed investigations of glass composition to discard analyses that represent bias data due to microlite composition.

The purpose of analysing chemical composition of pumice and scoria peaks is to precisely identify the chemical composition of tephra along the core in order to compare them with those of on-land products known for recent Montagne Pelée activity (Westercamp and Traineau, 1983b; Fichaut et al., 1989). No data has been acquired on lava dome clasts since they are too microcrystallized.

4. Results

5.1. Core description

Cores from hole U1401A, 15.61 m long, were described using core logs and photos obtained on-board during the cruise. The close-up photograph of the section U1401A-1H and a synthetic core description of the whole core are presented in Fig. 2. It consists of a series of volcanoclastic sediments intercalated in hemipelagic mud made of silt and clays (Fig. 2a). We can distinguish two types of volcanoclastic deposits: volcanoclastic turbidity deposits and tephra layers.

Turbidity deposits are a few tens of centimeters to several meters thick. They are of dark color, massive or normally graded, with various grain-sizes depending on the position in the core. 10 turbidity deposits are present in the core, named T1 to T10, from top to bottom (Fig. 2a, b). In the upper part of the core down to 5 m, turbidity deposits are few, thin, fine-grained and massive, with thickness ranging from 15 cm to 130 cm. The upper one, T1, is 50 cm

thick, massive and dark deposit at the top of the core. It covers unconsolidated brown hemipelagic mud which corresponds to the recent hemipelagic mud observed generally at the top of cores. Below 5 m, turbidity deposits are thicker, coarse-grained, normally graded and more abundant. Below 10 m, the whole core is made of turbidity deposits without intercalated hemipelagic mud. The last four turbidity deposits (T7 to T10) are significant not only for their thickness but also for their grain-size. These turbidity deposits are normally graded, with large size particles (up to 5 cm) at the bottom and small size particles at the top.

24 tephra layers were identified in the first 8 m of the core. They are of dark color, sandy, a few cm thick, mainly interbedded in hemipelagic levels or more rarely in turbidity deposits. In the lower part of the core, tephra layers are scarce or totally absent.

19 levels of hemipelagic sediments can be recognized in the first 10 m (Fig. 2a, b); they have clear sand color and thickness ranging from ~2-6 cm to ~70 cm. They are usually deformed or distorted, probably due to coring effects.

5.2. Physical properties analyses

Results from magnetic susceptibility and GRA (Gamma Ray Attenuation) density evidence adequate correlations between the two sets of values (Fig. 3). Turbidity deposits exhibit important variations in magnetic susceptibility (2500 to 4000 $*10^{-5}$ SI) and GRA density (0.5 to 2 g/cm^3) (Fig. 3a). This is likely related to the coarse-grained characteristic of the basal part of the turbidity deposits leading to the poor ability of large size particles to ensure compaction and a lack of mineralogical sorting. Hemipelagic sediments show the largest amplitude in variations in physical properties with low values of about 1000-1500 $*10^{-5}$ SI for magnetic susceptibility and < 1.5 g/cm^3 for GRA density (Fig. 3a). A detailed view of section U1401A-1H2 (Fig. 3b) enables us to precisely analyze magnetic susceptibility

variations at a centimeter scale. Six negative peaks are identified for hemipelagic parts of the section, one main positive peak for turbidity deposit and six correspond to thin tephra layers (Fig. 3b).

5.3. Lithology

Counting of 46 samples of tephra layers and turbidity deposits along the core were performed in order to characterize the lithological composition of the different volcanoclastic deposits (Fig. 2b). The most representative type of particles in the tephra layers are lava dome clasts. 16 different peaks can be recognized and their abundance is mostly higher than 30%, with maximum values at about ~96%.

Abundance of pumice clasts ranges from 0 to 95% all along the core. 6 pumiceous peaks can be identified: 4 in the shallow part of the core with pumice content of 88-95 % (at a depth of 95, 163, 240 and 300 cm respectively) and 2 in its deeper part (at a depth of 700 and 800 cm) showing pumice percentages of less than 50%. Scoria clasts are in low abundance (10-15%) except for three scoria peaks (45-60%) at a depth of 688, 713 and 766 cm. Lithology of the major volcanoclastic turbidity deposits is dominated by lava dome clasts (80 to 98 %).

5.4. $\delta^{18}O$ stratigraphy and ^{14}C dating

$\delta^{18}O$ analyses on planktonic foraminifera (*Globigerinoides ruber* - white) of hemipelagic sediments exhibit fluctuations ranging from -2.52‰ (at 286 cm depth) to a maximum value of 0.07‰ (at 650 cm depth; Fig. 2c). 3 remarkable points were chosen for ^{14}C dating (red dots in Fig. 2c) : a steep negative peak of - 0.75‰ (at 290 cm depth), the maximum positive peak of 0.07‰ (at 650 cm depth) and the final last hemipelagic layer of the core of -0.60‰ (at 965

cm depth). For these three points, ^{14}C dating returned estimated ages of 8082 ± 86 years cal. BP, 24677 ± 172 years cal. BP and 36425 ±191 years cal. BP respectively (after calibration with intcal 09.14c, Reimer et al, 2009).

5.5. SEM observations

Textures of pumice, scoria and lava dome clasts were obtained by BSE imaging (Fig. 4). Clasts present large differences in size, shape and vesicularity. Lava dome clasts (Fig. 4a) are poorly vesiculated, with highly microcrystallized matrix glass. On the contrary, pumice clasts (Fig. 4b) are vesiculated with glassy matrix glass and thin bubble walls. Scoria clasts (Fig. 4c) are moderately vesiculated, with more contorted vesicle shape, larger bubble walls and more microcrystallized matrix glass than in pumice clasts.

5.6. Geochemistry

Major element compositions were measured in the main pumiceous and scoriaceous tephra layers and their matrix glasses exhibit few variations in composition (Table 1). For pumice clasts, silica content is centered at rhyolitic values of about 73-78 wt% SiO_2 (Fig. 5a) with a total alkali content of about 5 wt%. Contrariwise, scoria clasts from tephra layers and turbidity deposits (T8, T9 and T10) show an extended compositional variability from andesite (67 wt% SiO_2) to rhyolite (74 wt% SiO_2) with 6-7 wt% alkali content (Fig. 5a).

5. Discussion

374 *6.1. Marine chronostratigraphic framework of the core U1401A*

375

376 The chronostratigraphical record of core U1401A is first compared to a previous well-
377 established tephrochronological one from a deep-sea sediment core CAR-MAR 4, collected
378 50 km northwest and downwind off Martinique Island (Fig. 1b) during the CARAVAL cruise
379 in 2002 (Boudon et al., 2013). This core is in a steadier environment for sedimentation than
380 that of the core U1401A, on a high point and outside the flow zones of debris avalanche and
381 turbidity currents. For these reasons it may be used as a reference for our tephrochronological
382 study in order to estimate the time period registered by the core U1401A. As the base of the
383 core U1401A is located on the roof of the debris avalanche deposit related to the third flank
384 collapse of Montagne Pelée, the tephrochronogical investigations will also provide constrains
385 on a minimum age of the flank collapse.

386 CAR-MAR 4 is a 10.6 m long core, characterized, from top to bottom, by 7 m of
387 continuous sedimentation with thick hemipelagic layers, tephra layers and no turbidity
388 deposits followed by 3.6 m of disturbed and unstructured sedimentation (Boudon et al., 2013).
389 Only the first 7 meters were investigated for tephrochronological studies. CAR-MAR 4 $\delta^{18}O$
390 results have already been correlated with a well-dated nearby deep-sea core (EN32-PC6,
391 Broecker et al., 1990). The correlation shows that CAR-MAR 4 covers the last 32 cal. ka BP
392 (Fig. 6). We can use it as a reference curve for U1401A because the two cores are spatially
393 close and analyses have been realized on the same planktonic foraminifera species and with
394 the same analytical protocol for both. Owing to the presence of thick turbidity deposits in the
395 core U1401A, to establish an adequate correlation with the CAR-MAR 4 $\delta^{18}O$ curve, it is
396 necessary to subtract the thickness of the turbidity deposits. This allows us to obtain a real
397 chronostratigraphic scale for hemipelagic deposits.

A spectral analysis and a correlation between the two cores have been processed using the free software Analyseries (Paillard et al., 1996). This software enables us to compare our $\delta^{18}O$ data with the selected reference CAR-MAR 4 curve by selecting and comparing a series of calibration points between the two curves. From the calibration points, Analyseries realizes a linear intercalibration to calculate the age of the intermediate points of the curve. It takes into account the age and the depth of the two calibration points up and down the intermediary one, and the depth of the intermediary point, according to the equation:

$$Age_X = [(age_A - age_B) / (depth_A - depth_B)]*[depth_X - depth_A] + age_A$$

where X is the intermediary point, A the upper calibration point and B the lower calibration point.

In the final age model (Fig. 6), the two curves are correlated with a coefficient of 0.936 and correlation returns a mean pelagic sedimentation rate of 22cm/ka, consistent with that known for the Grenada basin (Reid et al., 1996; Boudon et al., 2007). From the modelled ages, the core U1401A covers a period from 0 to ~36 cal. ka BP, with a maximum $\delta^{18}O$ value (0.07 ‰) at about 25 cal. ka BP. The overlap of the two curves is clear especially in the first part (0-8 ka). However, for recent ages, a small shift is evident between the two cores (Fig. 6): the modelled ages of the core U1401A are younger than those of CAR-MAR 4. This proves that the core U1401A recorded the largest temporal range, probably because of the presence of a thick turbidity deposit (T1, 50 cm thick) at the top of the core that allowed the preservation of the youngest and not compacted sediments, usually destroyed by drilling processes.

Another difference between the two cores is the sampling frequency used for $\delta^{18}O$ chronostratigraphy. The sampling interval for the core CAR-MAR 4 is constant at 10 cm while the sampling interval could not be kept constant for the core U1401A. Sampling the core U1401A led to two types of problems: (1) the presence of numerous and thick turbidity

423 deposits and (2) the low content of the planktonic foraminifera *Globigerinoides ruber* in
424 many samples. These problems can be explained by the particular position of the U1401 site,
425 located on the submarine flank of the volcano. As a result the site is more exposed to clastic
426 and clayey sedimentation related to on-land processes, which induce a decrease in biogenic
427 steady-state sedimentation. Secondly, the presence of thick turbidity deposits has a significant
428 impact on the sedimentary record of U1401A core. The correlation between the two cores is
429 lost when turbidity deposits are present (Fig. 6). In fact, some significant gaps occur, causing
430 a lack of thousands of years in the sedimentary record. A strong erosive power of turbidites
431 can probably be invoked during their deposition process.

432 Three ^{14}C dates were performed to obtain absolute ages on 3 key positions of the
433 U1401A core (Figs 2c, 6). They are roughly located at the top, the center and the bottom of
434 the core (respectively at 197, 348.5 and 488.5 cm turbidity deposits off depths). These 3
435 points have been selected as they represent a particular milestone in the evolution of the $\delta^{18}O$
436 curve. In addition, dating the top and bottom of the curve allows us to obtain the entire
437 coverage period of the core and an absolute age for the sediments located on the DAD. The
438 most recent age obtained (8220 cal. ka BP) is well consistent with the model obtained with
439 $\delta^{18}O$ analysis. It corresponds to a positive peak in the $\delta^{18}O$ record. The second ^{14}C age of
440 24677 cal. ka BP corresponds to the higher value of the $\delta^{18}O$ obtained in the core U1401A. If
441 we compare with the CAR-MAR 4 curve where the higher value of the $\delta^{18}O$ curve is obtained
442 at a more recent age (~18 ka), the maximum value of the U1401A $\delta^{18}O$ curve is probably too
443 high (Fig. 6a). This is likely related to the lack of points in the $\delta^{18}O$ record due to the erosion
444 by turbidity density currents during the 17-24 ka period where the maximum $\delta^{18}O$ value is
445 reached. The third ^{14}C age of 36425 cal. ka BP corresponds to the lowest point sampled in a
446 small hemipelagic deposit interbedded between T7 and T8 turbidity deposits and overlaying
447 the top of the debris avalanche deposit (T8 to T10) of the U1401A core. As this third age is

448 obtained on the lowest hemipelagic level of the core but not really at its physical bottom, our
449 results of ~36 cal. ka BP represents a minimum age for the occurrence of the third flank
450 collapse of Montagne Pelée, that significantly contrasts with what was thought up to now.
451 Nevertheless below this point three thick turbidity deposits (T8 to T10) are present. They
452 overly the top of the debris avalanche deposit. No hemipelagic sediments are identified
453 between these turbidity deposits or at the top of the debris avalanche deposit. These
454 observations lead us to believe that it is likely that turbidity deposits T8 to T10 formed in a
455 short period of time directly after the flank collapse event.
456
457 *6.2. Tephrochronology, stratigraphy and eruptive styles*
458
459 Figure 7 shows the complete estimated chronostratigraphic model of the core U1401A.
460 24 tephra layers and 10 turbidity deposits have been recognized all along the core by cross
461 correlation of photos observations, counting techniques and analysis of physical properties.
462 The comparison of tephra record between the core U1401A and the core CAR-MAR 4 is
463 showed in Figure 6.
464 The core U1401A can be divided in three different units. In the first unit, 0-3 m in depth
465 (0 to 9 cal. ka BP), 2 turbidity deposits can be recognized (Fig. 7, T1= 50 cm and T2= 10 cm).
466 The first turbidity deposit (T1) is located at the top of the core, covering the recent and not
467 compacted hemipelagic sediments. Its peculiar position allows it to be linked to the last period
468 of volcanic activity characterized by the last 1902-1905 and 1929-1932 dome-forming
469 eruptions. In addition, its lithology (prevalence of lava dome's clasts) is similar to that of on-
470 land pyroclastic density current deposits (Bourdier et al., 1989). This unit is also characterized
471 by the occurrence of 10 tephra layers (Fig. 7, red lines = 4 pumice clast-rich levels and blue
472 lines = 6 lava dome clast-rich levels) interbedded in the hemipelagic sedimentation. Such

alternation of pumice clasts and lava dome clasts-rich levels is consistent with tephrochronological results on the core CAR-MAR 4 (Fig. 6b, Boudon et al., 2013) and with observations on on-land deposits that show the well-known alternation between dome-forming eruptions and plinian or subplinian eruptions (P1 to P8 eruptions, Westercamp and Traineau, 1983a, b; Traineau et al., 1989 Michaud-Dubuy, 2019). The residual glass of the pumice clasts from these tephra layers has rhyolitic composition (about 75 wt% SiO_2 and 5 wt% Na_2O+K_2O) which is close to the composition of the residual glass of the pumice clasts from on-land deposits (Fig. 5b). Furthermore their composition is clearly far from that of Dominica island (SiO_2 ~78 wt%, Na_2O+K_2O ~5-7 wt%, Balcone-Boissard et al., 2018) and clearly excludes tephra originating from Dominica volcanoes, even though more investigations have to be performed using trace elements proxies. We see that the record of eruptive events is lower in the core U1401A than for the core CAR MAR4 and also for on-land record (Fig. 6). This is due to the location of the site U1401 not in the axis of the main local windward direction of the winds (westbound trade) and to the dispersion of the plumes from plinian and subplinian eruptions or ash-clouds associated to block- and ash pyroclastic density currents.

The second unit of the core, 3 to 8 m in depth (9 to 30 cal. ka BP) is characterized by well-spaced turbidity deposits (Fig. 7, T3 to T6) in thick hemipelagic layers. Their thickness varies from 10 cm (T4) to 120 cm (T5). Lithology of T3 and T5 shows the prevalence of lava dome's clasts; they are probably linked with block- and ash pyroclastic density currents associated to dome-forming eruptions. A total of 14 tephra layers can be documented in this unit. Only 3 tephra layers enriched in lava dome clasts are recognized in the first half of the second unit (Fig. 7, blue lines) whereas 11 tephra layers are present in the second half. 6 of them are rich in dome clasts (blue lines), 2 rich in pumice clasts (red lines), whereas 3 of them contain scoria clasts (green lines). In these tephra, the residual glass of scoria clasts is more

498 basic than the residual glass of the pumice clasts (~65 wt% SiO_2, Fig. 5a), but we also
499 observed some clasts that exhibit a more evolved composition (~75 wt% SiO_2) – see
500 explanation in the next section. The lack of tephra records between 5 and 6.7 m in this unit
501 may be related to a decrease in volcanic activity, or the set-up of thick turbidity deposits that
502 eroded a part of the previously deposited sediments.

503 The third unit of the core, 8 to 15 m in depth (30 to 36 cal. ka BP) is almost exclusively
504 characterized by thick turbidity deposits (T7 to T10). Their thickness varies from 140 cm (T7)
505 to 230 cm (T8). Lithological results highlighted that these turbidity deposits are rich in lava
506 dome's clasts but also in scoria clasts (about 10 to 20 %). The absence of hemipelagic
507 sediments in this part of the core indicates a significant supply of volcanic products in a short
508 time interval.

509

510 *6.3. Origin of the scoria-rich levels*

511

512 Complete results on U1401A core show that the turbidity deposits and some of the tephra
513 layers from the bottom of the core are rich in scoria clasts (up to 60% of the clasts in the
514 sections between 680 and 820 m depth) of more basic composition (~65 wt% SiO_2). The
515 proportion of scoria clasts decreases progressively to the top of the core rarely being over a
516 background content of 5% of clasts.

517 Based on tephrochronological study of the CAR-MAR 4 core (Fig. 6b) and on-land data,
518 Boudon et al. (2013) have proposed that abundant deposits of scoria flows of basaltic
519 andesitic composition were generated after the second flank collapse event, estimated around
520 32 ka, whereas acid andesitic magma were emitted before this flank collapse event. These
521 changes in composition and eruptive style are explained by the decrease of the threshold
522 effect exerted by the volcanic edifice on the magma plumbing system allowing more basic

523 and denser magmas to reach the surface (Pinel and Jaupart, 2005; Boudon et al., 2013,
524 Cassidy et al., 2015). This activity occurred over several thousand years, rapidly building a
525 new cone inside the horseshoe-shaped structure. This also shows that the magma production
526 was high just after the flank collapse and gradually decreased during the building of the new
527 cone and progressively exerted a new threshold effect on the plumbing system. The magma
528 production is then probably reduced for a few thousand years before resuming with the
529 production of more acidic and less dense magmas. The ages proposed for this period of
530 basaltic andesite emissions range between 32 cal. ka BP or more and 27 cal. ka BP. A period
531 of weaker magmatic activity occurs between 27 to 22.5 cal. ka BP prior to a new emission of
532 andesites from 22.5 cal. ka BP to present (Boudon et al., 2013).

533 The on-land relationship between the horseshoe-shaped structure of the second flank-
534 collapse and the scoria pyroclastic density currents were not clearly established as the scoria
535 pyroclastic density currents which resulted from column collapse of explosive eruptions,
536 covered all the flanks of the volcano inside and outside the horseshoe-shaped structures.

537 Considering 1) the estimated ages of the on-land scoria pyroclastic density currents
538 (Westercamp and Traineau, 1983a, b), the age of the tephra levels rich in scoria clasts in the
539 CAR-MAR 4 core band the ages obtained on the turbidity deposits and tephra level rich in
540 scoria clasts of the U1401A core; 2) the similar composition of the residual glass of these
541 scoria clasts in the cores and on-land, we can assume that all these deposits belong to the
542 same period of activity of Montagne Pelée and the production of basaltic andesites during this
543 period did not follow the second but the third flank collapse as the site U1401 is located on
544 the third DAD.

545 We also observe that even if the emitted magmas are dominantly basaltic andesites, they
546 can be associated with more evolved magmas of dacitic composition with rhyolitic glasses
547 (Fig. 5). This characteristic has already been evidenced on-land for these eruptions (Traineau

et al., 1983; Bourdier et al., 1985) and explained by the presence of more superficial and small pocket of more evolved magmas within the "mushy" plumbing system impacted by the ascent of more basic magmas stored deeper (Pichavant et al., 2002). This magma mixing generally occurred at the beginning of the eruptive phases.

5.4. Age of the third flank collapse and relationship with the volcanic activity

Our results allow us to propose a significant shift in age of the third flank collapse from 9 ka to ~36 cal. ka BP.

Considering that the drilling operations of the core U1401A reach the top of the third DAD, and on the basis of the $\delta^{18}O$ age model and on the ^{14}C ages we can consider that the age of 36425 ± 191 cal. ka BP obtained in the lowest level of hemipelagic mud is a minimum age for the third DAD and the corresponding flank collapse. But a series of turbidity deposits (T8 to T10) are recognized between the last dated hemipelagic mud and the top of the debris avalanche deposits. Thus it is possible to raise the question of the time interval separating this ^{14}C age from the true age of the flank collapse.

As previously proposed, the decrease of the load exerted by the third flank-collapse has led to the production of scoria rich deposits of basaltic composition and to a high magma production rate. This high magma production rate generated abundant scoria pyroclastic density currents that entered the sea and evolved in turbidity currents. This explains the abundance and the thickness of the turbidity deposits recognized at the base of the U1401A core and on the debris avalanche deposit. This abundance of volcanic products generated after the flank-collapse supports rapid deposition from the turbidity currents (T8 to T10). We can consider that the time between the flank collapse and the ascent of more basic magmas is not too long (probably not more than a few decades) and that the age of 36.425 cal. ka BP

obtained on the hemipelagic mud covering these turbidity deposits is a minimum age not so far from the true age of the debris avalanche setup.

5.5. The recent eruptive history of Montagne Pelée

Previous studies have described the eruptive history of Montagne Pelée as the succession of three different phases of construction of the volcanic edifice, separated by two flank collapses (Fig. 8a); the third flank collapse, is in fact included in the third stage of building (Le Friant et al., 2003; Boudon et al., 2005, 2007, 2013; Germa et al., 2011a). On the basis of on-land studies, the three different flank collapses had previously been dated at 127 ka (Germa et al., 2011a) for the first one, 32 ka (Boudon et al., 2013) and 9 ka (Le Friant et al., 2003), respectively for the second and the third one.

Nevertheless, the results of our study significantly modify the volcanological evolution of Montagne Pelée and allow us to submit a new evolution for the volcano (Fig. 8b). On-land, several rims of flank collapse structures have been identified (Fig. 11 of Le Friant et al., 2003 and Fig 1c). The rims resulting from the first flank-collapse structure are clearly identified, though its southern rim is not visible as it is covered by the products of the most recent volcano activity. Rims of the third flank collapse structures are clearly identifiable as they are the most recent, but they are also partially covered by recent volcanic products. On the contrary, the scars originating from the second flank collapse structure are not clearly visible and remain questionable on the basis of on-land investigations. Recent offshore studies following the IODP expedition 340 have shown that the DADs do not have the extension previously proposed (Le Friant et al., 2015; Brunet et al., 2016). The large chaotic deposits identified on seismic profiles and on bathymetry are deformed sediments pushed by the DAD that stopped at the base of the submarine flank. It is difficult to distinguish the DADs of the

598 first and the second event because they form a unique bulge at the base of the submarine flank
599 of the volcano (Fig 1b). On the contrary, the third DAD is clearly identified on the submarine
600 flank of the volcano with its lobe-shape and its hummocky morphology.

601 The question of the occurrence of three flank collapse events can thus be addressed in a
602 serious manner. The morphology and the distribution of the valleys indicate that the northern
603 rim of the first flank collapse structure exists. Its age of 127 ka (Germa et al., 2011a) obtained
604 on two lava domes on each part of the rim is reliable. The third flank collapse is now also
605 clearly identified by the presence of submarine DADs, some remnants of hummock
606 morphology on-land and the rims of the horse-shoe shaped structure (Le Friant et al., 2003).
607 Its age is now confidently set at ~36 ka (this study). The time interval that separated the first
608 (127 ka) from the third flank collapse (~36 ka) is in the order of 90 ka. Is this short period
609 enough to build a new cone destroyed by a second flank collapse and a third cone destroyed
610 again by the third one? It is difficult to answer this question as the data we produce in this
611 study concern the last 40 000 thousand years. However the magma production rate of
612 Montagne Pelée is, although significant, not very high and can be estimated at a few km^3/10
613 000 years for the last tens of thousands of years (Wadge, 1984, Michaud-Dubuy, 2019). We
614 can consider that the highest magma production rate occurred after the flank collapse event
615 dated now at ~36 ka over a period of 10 000 years. An alternative to the already proposed
616 evolution of the volcano - that must be confirmed by on-land work and additional
617 tephrochronological investigations on other marine cores in the period between the first and
618 the "third" flank collapse - is that only two flank collapses occurred (Fig. 8b): the first one
619 at127 ka, and the last one at 36 ka. Though less voluminous, this last flank-collapse modified
620 the dynamics of the magmatic plumbing system, leading for a short period of time to the
621 ascent of more basic and denser magma than those emitted before the flank collapse.
622 Following this flank collapse, a lot of explosive eruptions produced scoria fall and density

currents covering a large part of the volcano. Numerous turbidity currents were generated by scoria density currents entering into the sea or by the remobilization of scoria density current deposits, covering part of the submarine flank of Montagne Pelée. The eruptive activity was high just after the flank-collapse and decreased progressively. The significant eruptive activity rapidly involved the building of a new volcanic edifice which exerted a new threshold effect on the plumbing system. The volcanic activity decreased and progressively a change in the composition of the emitted magmas occurred; more acidic magmas were generated giving rise to the alternance of plinian or subplinian events and dome-forming eruptions up to this day.

6. Conclusions

The detailed study of the core U 1401a located on the submarine flank of Montagne Pelée, on the hummocky deposit of the third debris avalanche (DAD 3) has improved our knowledge of the eruptive history. It has allowed us to propose a minimum age of ~36 ka for the last flank collapse. It also indicates that the volcanic activity can be modified in terms of magma production and in terms of magma composition after a flank collapse. Deeper and more basic magmas can erupt for a long time before a new cone exerts a threshold effect on the plumbing system, reducing the magma production rate and changing the composition of the emitted magmas. It also indicates that after a flank collapse, a lot of turbidity currents can occur resulting in the offshore evolution of abundant pyroclastic density currents or the remobilization of on-land deposits. It also shows that a sole core does not enable the reconstruction of all the eruptive history of a volcano for a given period. The core U1401 located on the western submarine flank of Montagne Pelée is well located for the study of the post flank-collapse activity and the pyroclastic density currents as well as tephra layers.

Abundant turbidity deposits have an significant erosive power, destroying part of the lower deposits, but can also preserve recent and not compacted hemipelagic sediments, generally not observed, as was the case for the upper recent turbidity deposits. The core CAR MAR 4 is best located to study tephra layers as it is on a high point without erosion and closer to the direction of the winds (East-West) in the troposphere. But a lot of tephra are dispersed to the East as the eruptive column for Plinian eruptions reaches the stratosphere where the wind direction is generally West-Easterly. A core located to the east of Montagne Pelée will allow us to complete the eruptive history of the volcano.

……

Acknowledgments

We thank the captains, officers, crews of the R/V Joides Resolution and the IODP-340 scientific mission. Major element analyses at the microprobe facility benefited the support of M. Fialin and N. Rividi (Service CAMPARIS). Oxygen stratigraphy analysis benefited the support of N. Labourdette (UPMC). Imaging at SEM was helped by Omar Boudouma (Sorbonne Université). We thank INSU, NERC, ANR-13-BS06-0009 for funding. ^{14}C dating were performed at LMC14 laboratory (Artemis program). We also thank E. Lebas for her participation and help in the acquisition of planktonic foraminifera samples.

References

672 Allan, A.S.R., Baker, J.A., Carter. L., Wysoczanksi, R.J., 2008. Reconstructing the
673 Quaternary evolution of the world's most active silicic volcanic system: insights from an
674 ~1.65 Ma deep ocean tephra record sourced from Taupo Volcanic Zone, New Zealand.
675 Quat. Sci. Rev. 27(25–26): 2341–2360.
676 Balcone-Boissard, H., Boudon, G., Blundy, J.D., Martel, C., Brooker, R.A., Deloule, E.,
677 Solaro, C., Matjuschkin, V., 2018. Deep pre-eruptive storage of silicic magmas feeding
678 Plinian and dome-forming eruptions of central and northern Dominica (Lesser
679 Antilles) inferred from volatile contents of melt inclusions Contrib. Mineral. Petrol.
680 173:101, https://doi.org/10.1007/s00410-018-1528-4.
681 Boudon, G., Lajoie, J., 1889. The 1902 péléean deposits in the Fort Cemetery of St. Pierre,
682 Martinique: a model for the accumulation of turbulent nuées ardentes. In: Boudon, G.,
683 Gourgaud, A. (Eds), Montagne Pelée. J. Volcanol. Geotherm. Res. 38:113-129.
684 Boudon, G., Le Friant, A., Villemant, B., Viodé, J.-P., 2005. Martinique. In: Lindsay, J.M.,
685 Robertson, R.E.A., Shepherd, J.B., Ali, S. (Eds.), Volcanic Atlas of the Lesser Antilles.
686 Seismic Research Unit, The University of the West Indies, Trinidad and Tobago, WI,
687 pp 65–102.
688 Boudon, G., Le Friant, A., Komorowski, J.-C., Deplus, C., Semet, M.P., 2007. Volcano flank
689 instability in the Lesser Antilles Arc: diversity of scale, processes, and temporal
690 recurrence. J. Geophys. Res. 112, B08205.
691 Boudon, G., Villemant, B., Le Friant, A., Paterne, M., Cortijo, E., 2013. Role of large flank
692 collapses on magma evolution of volcanoes. Insights from the Lesser Antilles Arc. J.
693 Volcanol. Geotherm. Res. 263:224-237. http://dx.doi.org/10.1016/j.jvolgeores.
694 2013.03.009.

695 Bourdier, J.-L., Gourgaud, A., Vincent, P.M., 1985. Magma mixing in a main stage of
696 formation of Montagne Pelée: the Saint Vincent-type scoria flow sequence (Martinique,
697 F.W.I.). J. Volcanol. Geotherm. Res. 25:309-332.

698 Bourdier, J.-L., Boudon, G., Gourgaud, A., 1989. Stratigraphy of the 1902 and 1929 nuée
699 ardente deposits, Montagne Pelée, Martinique. In: Boudon, G., Gourgaud, A. (Eds):
700 Mount Pelée. J. Volcanol. Geotherm. Res. 38:77-96.

701 Bouysse, P., Westercamp, D., Andreieff, P., 1990. The Lesser Antilles Island Arc.
702 Proceedings of the Ocean Drilling Program, Part B: Scientific Results 110:29–44.

703 Broecker, W.S., Klas, M., Clark, E., 1990. Accelarator mass spectroscopic radiocarbon
704 measurements on foraminifera shell from deep-sea cores. Radiocarbon 32(2):119-133,

705 Brunet, M., Le Friant, A., Boudon, G., Lafuerza, S., Talling, P., Hornbach, M., Ishizuka, O.,
706 Lebas, E., Guyard, H. and IODP Expedition 340 science Party, 2016. Composition,
707 geometry, and emplacement dynamics of a large volcanic island landslide offshore
708 Martinique: From volcano flank-collapse to seafloor sediment failure? Geochem.
709 Geophys. Geosyst .16, doi:10.1002/2015GC006034.

710 Cassidy, M., Watt, S.F.L., Talling, P.J., Palmer, M.R., Edmonds M., Jutzeler, M., Wall-
711 Palmer, D., Manga, M., Coussens, M., Gernon, T., Taylor, R.N., Michalik, A., Inglis,
712 E., Breitkreuz, C., Le Friant, A., Ishizuca, O., Boudon, G., McCanta, M.C., Adachi, T.,
713 Hornbach, M.J., Colas, S.L., Endo, D., Fujinawa, A., Kataoka, K.S., Maeno, F.,
714 Tamura, Y., Wang, F., Ishizuka, O., and Shipboard Science Party, 2015. Rapid onset of
715 mafic magmatism facilitated by volcanic edifice collapse. Geophys. Res. Lett. 42,
716 4778–4785, doi:10.1002/2015GL064519.

717 Coussens, M., Wall-palmer, D., Talling, P.T., Watt, S.F.L., Cassidy, M., Jutzeler, M., Clare,
718 M.A., Hunt, J.E., Manga, M., Gernon, T.M., Palmer, M.R., Hatter, S.J., Boudon, G.,

719 Endo, D., Fujinawa, A., Hatfield, R., Hornbach, M.J., Ishizuka, O., Kataoka, K., Le
720 Friant, A., Maeno, F., McCanta, M., Stinton, A.J., 2016. The relationship between
721 eruptive activity, flank collapse, and sea level at volcanic islands: A long-term (>1 Ma)
722 record offshore Montserrat, Lesser Antilles. Geochem. Geophys. Geosyst.,
723 doi:10.1002/2015GC006053.

724 Deplus, C., Le Friant, A., Boudon, G., Komorowski, J.-C., Villemant, B., Harford, C.,
725 Ségoufin, J., Cheminée, J.-L., 2001. Submarine evidence for large-scale debris
726 avalanches in the Lesser Antilles Arc. Earth. Planet. Sci. Lett. 192:145-157.

727 D'Orbigny, A.D. 1839. Foraminifères, in de la Sagra R., Histoire physique, politique et
728 naturelle de l'ile de Cuba.Arthus Bertrand, Paris 224p.

729 Engwell, S.L., Sparks, R.S .J., Carey S. 2014. Physical characteristics of tephra layers in the
730 deep sea realm: the Campanian Ignimbrite eruption. In: Austin, W. E. N., Abbott, P. M.,
731 Davies, S. M., Pearce, N. J. G., Wastegard, S. (Eds). Marine Tephrochronology. J. Geol.
732 Soc. London, Special Publication, 398, 47–64. http://dx.doi.org/10.1144/SP398.7.

733 Fichaut, M., Marcelot, G., Clocchiatti, R. 1989. Magmatology of Mt. Pelée (Martinique,
734 F.W.I.). II: petrology of gabbroic and dioritic cumulates. In: Boudon, G., Gourgaud, A.
735 (Eds): Mount Pelée. J. Volcanol. Geotherm. Res. 38:171-18.
736 https://doi.org/10.1016/0377-0273(89)90036-X

737 Germa, A., Quidelleur, X., Lahitte, P., Labanieh, S., Chauvel, C., 2011a. The K–Ar
738 Cassignol-Gillot technique applied towestern Martinique lavas: A record of Lesser
739 Antilles arc activity from 2 Ma to Mount Pelée volcanism. Quaternary Geochronology
740 6:341–355.

741 Germa, A., Quidelleur, X., Labanieh, S., Chauvel, C., Lahitte, P., 2011b. The volcanic
742 evolution of Martinique Island: Insights from K–Ar dating into the Lesser Antilles arc
743 migration since the Oligocene. J. Volcanol. Geotherm. Res. 208:122-135.

744 Hughen et al., 2004. Marine 04 marine radiaacarbon age calibration, 0-26 cal kyr BP.
745 Radoicarbon 46:1059-1086.

746 Jenning, A., Thordarson, T., Zalzal, K., Stoner, J., Hayward, C., Geirsdotti, A., Miller, G.,
747 2014. Holocene tephra from Iceland and Alaska in SE Greenland Shelf Sediments. In:
748 Austin, W. E. N., Abbott, P. M., Davies, S. M., Pearce, N. J. G., Wastegard, S. (Eds).
749 Marine Tephrochronology. J. Geol. Soc. London, Special Publication, 398, 157-193.
750 http://dx.doi.org/10.1144/SP398.6.

751 Kutterolf, S., Schindlbeck, J. C., Robertson, A. H. F., Avery, A., Baxter, A. T., Petronotis, K.,
752 &Wang, K.-L. (2018). Tephrostratigraphy and provenance from IODP Expedition 352,
753 Izu-Bonin arc: Tracing tephra sources and volumes from the Oligocene to recent.
754 Geochemistry,Geophysics,Geosystems,19,150–174.
755 https://doi.org/10.1002/2017GC007100

756 Labanieh. S., Chauvel, C., Germa, A., Quidelleur, X., Lewin, E., 2010. Isotopic hyperbolas
757 constrain sources and processes under the Lesser Antilles arc. Earth. Planet. Sci. Lett.
758 298:35-46.

759 Lacroix, A., 1904. La Montagne Pelée et ses Eruptions. Masson ed., Paris, 662 pp.

760 Le Friant, A., Boudon, G., Deplus, C., Villemant, B., 2003. Large scale flank-collapse during
761 the recent activity of Montagne Pelée, Martinique, FWI. J. Geophys. Res. 108, B1, 2055.
762 Le Friant, A., Lock, E.J., Hart, M.B., Boudon, G., Sparks, R.S.J., Leng, M.J., Smart, C.W.,
763 Komorowski, J.-C., Deplus, C., Fisher, J.K., 2008. Late Pleistocene tephrochronology

764 of marine sediments adjacent to Montserrat, Lesser Antilles volcanic arc. J. Geol. Soc.
765 London165:279–289.

766 Le Friant, A. et al., 2015. Submarine record of volcanic island construction and collapse in
767 the Lesser Antilles arc: First scientific drilling of submarine volcanic island landslides
768 by IODP Expedition 340. Geochem. Geophys. Geosyst. 16:420-442.
769 doi:10.1002/2014GC005652.

770 Lowe, D.J., 2014. Marine tephrochronology: a personal perspective. In: Austin, W. E. N.,
771 Abbott, P. M., Davies, S. M., Pearce, N. J. G., Wastegard, S. (Eds). Marine
772 Tephrochronology. J. Geol. Soc. London, Special Publications, 398, 7-19.
773 http://dx.doi.org/10.1144/SP398.11.

774 Martin-Kaye, P.H.A., 1969. A summary of the geology of the Lesser Antilles. Overseas
775 Geology and Mineral Resources 10(2):172–206.

776 Michaud-Dubuy, A., 2019. Dynamique des éruptions pliniennes : réévaluation de l'aléa
777 volcanique en Martinique. Thèse Université de Paris, 200 pp.

778 Paillard, D., Labeyrie, L., Yiou, P., 1996. Macintosh program performs time-series analysis.
779 Eos, Transactions, Am. Geophys. Union, 77:379 (Abstract).

780 Paterne, M., Guichard, F., Labeyrie, J. 1988. Explosive activity of the SouthItalian volcanoes
781 during the past 80000 years as determined by marine tephrochronology. J. Volcanol.
782 Geotherm Res., 34:153–172, http://dx.doi.org/10.1016/0377-0273(88)90030-3.

783 Paterne, M., Labeyrie, J., Guichard, F., Mazaud, A., Maitre, F. 1990. Fluctuations of the
784 Campanian explosive volcanic activity South Italy during the past 190,000 years, as
785 determined by marine tephrochronology. Earth Planet. Sci. Lett., 98:166–174,
786 http://dx.doi.org/10.1016/0012-821X(90)90057-5

787 Paterne, M., Guichard, F., Duplassy, J.-C., Siani, G., Sulpizio, R., Labeyrie, J., 2008. A
788 90,000–200,000 yrs marine tephra record of Italian volcanic activity in the Central
789 Mediterranean Sea. J. Volcanol. Geotherm. Res. 177:187–196.

790 Perret, F., 1937. The Eruption of Mt. Pelée 1929-1932. Carnegie Inst. Washington, Publ. 458,
791 126 pp.

792 Pichavant, M., Martel, C., Bourdier, J., Scaillet, B. 2002. Physical conditions, structure, and
793 dynamics of a zoned magma chamber: Mount Pelée (Martinique, Lesser Antilles arc). J.
794 Geophys. Res. 107, doi:10.1029/2001JB000315.

795 Pinel, V., Jaupart. C., 2005. Some consequences of volcanic edifice destruction for eruption
796 conditions. J. Volcanol. Geotherm. Res. 145, 68-80.

797 Reid, R.P., Carey, S.N., Ross, D.R., 1996. Late Quaternary sedimentation in the Lesser
798 Antilles island arc. Geol.Spc. Am. Bull. 108:78-100.

799 Reimer, P.J. et al., 2009. IntCal09 and Marine09 radiocarbon age calibration curves, 0–50,000
800 years cal BP. Radiocarbon 51(4):1111-1150.

801 Roobol, M.J., Smith, A.L.,1976. Mount Pelée, Martinique: A pattern of alternating eruptive
802 slyles. Geology 4(9): 521-524.

803 Shane, P., 2000. Tephrochronology: a New Zealand case study.Earth-Science Reviews 49(1-
804 4): 223-259.

805 Shane, P., Sikes, E.L., Guilderson. T.P., 2006. Tephra beds in deep-sea cores off northern
806 New Zealand: implications for the history of Taupo Volcanic Zone, Mayor Island and
807 White Island volcanoes. J. Volcanol. Geotherm. Res. 154:276–290.

808 Sigurdsson, H., Carey, S.N., 1981. Marine tephrochronology and Quaternary explosive
809 volcanism in the Lesser Antilles arc. In: Self S., Sparks R.S.J. (eds) Tephra Studies.
810 Springer, Dordrecht, 75: 255-280.

811 Smith, A.L., Roobol, M.J., 1990. Mt Pelée, Martinique; A Study of an Active Island-arc
812 Volcano. Geol. Soc. Am. Memoir 175 105 p.
813 Talling, P., Masson, D.G., Sumner, E.J., Malgesini, G., 2012. Subaqueous sediment density
814 flows: Depositional processes and deposit types. Sedimentology 59(7):1937-2003.
815 Traineau, H., Westercamp, D., Coulon, C., 1983. Mélanges magmatiques à la Montagne Pelée
816 (Martinique). Origine des éruptions de type Saint-Vincent. Bull. Volcanol. 46 :243-269.
817 Traineau, H., Westercamp, D., Bardintzeff, J.-M., Miskovsky, J.-C., 1989. The recent
818 pumiceeruptions of Mt. Pelée volcano, Martinique. Part I: Depositional sequences,
819 description of pumiceous deposits. J. Volcanol. Geotherm. Res. 38:17-33.
820 Trofimovs, J., Amy, L., Boudon, G., Deplus, C., Doyle, E., Fournier, N., Hart, M.M.B.,
821 Komorowski, J.-C., Le Friant, A., Lock, E., Pudsey, C., Ryan, G., Sparks. R.S.J.,
822 Talling, P.J., 2006. Submarine pyroclastic deposits formed at the Soufrière Hills
823 Volcano, Montserrat (1995-2003): what happens when pyroclastic flows enter the
824 ocean? Geology, 34 (7):549-552.
825 Wadge, G., 1984. Comparison of volcanic production rates and subduction rates in the Lesser
826 Antilles and Central America. Geology 12:555–558. http://dx.doi.org/10.1130/ 0091-
827 7613
828 Wall-Palmer D., Coussens M., Talling P.J., Jutzeler M., Cassidy M., Marchant M. Palmer
829 M.R., Watt S.F.L., Smart C.W., Fisher J.K., Hart M.B., Fraass F., Trofimovs J., Le
830 Friant A., Ishizuka O., Adachi T., Aljahdali M., Boudon G., Breitkreuz C., Endo D.,
831 Fujinawa A., Hatfield R., Hornbach M.J., Kataoka K, Lafuerza S., Maeno F., Manga
832 M.,Martinez-Colon M., McCanta M., McManus J.,Morgan S., Saito T., Slagle A.,
833 Stinton A.J., Subramanyam K.S.V., Tamura Y., Villemant B., Wang F., 2014. Late
834 Pleistocene stratigraphy of IODP Site U1396 and compiled chronology offshore of

south and south west Montserrat, Lesser Antilles, Geochem. Geophys. Geosyst ., 15, doi: 10.1002/2014GC005402.

Wall-Palmer, D., Hart, M.B., Smart, C.W., Sparks, R.S.J., Le Friant, A., Boudon, G., Deplus, C., Komorowski, J.-C., 2012. Pteropods from the Caribbean Sea: variations in calcification as an indicator of past ocean carbonate saturation. Biogeosciences 9(1):309-315. doi: 10,5194/bg-9-309-2012.

Weller, D.J., Miranda, C.G., Moreno, P.I., Villa-Martínez, R., Stern, C.R. 2015. Tephrochronology of the southernmost Andean SouthernVolcanic Zone, Chile; Bull Volcanol. 77: 107 DOI 10.1007/s00445-015-0991-2

Westercamp, D., Traineau, H., 1983a. Carte géologique au 1/20 000 de la Montagne Pelée, avec notice explicative. In: B.R.G.M. (Ed.), Orléans.

Westercamp, D., Traineau, H., 1983b. The past 5,000 years of volcanic activity at Mt. Pelee martinique (F.W.I.): implications for assessment of volcanic hazards. J. Volcanol. Geotherm. Res. 17:159–185. http://dx.doi.org/10.1016/0377-0273(83)90066-5.

Westercamp, D., Pelletier, B., Thibault, P.-M., 1990. Carte géologique de la Martinique à 1/50 000 avec notice explicative. B.R.G.M. eds, Orléans.

Wulf, S. W., Kraml, M., Brauer, A., Keller, J., Negendanl, J. F. W. 2004. Tephrochronology of the 100 ka lacustrine sediment record of Lago Grande di Monticchio (southern Italy). Quarternary International, 122, 7–30, http://dx.doi.org/10.1016/j.quaint.2004.01.028

Figure captions.

Figure 1. a) Geodynamic setting of the Lesser Antilles volcanic arc; Predicted bathymetry from Smith and Sandwell (1997). Contour interval is 500 m; **b**) Swath bathymetry of the west coast of Martinique with the position of the bulge, the SLD and the

DAD 3. Contour interval is 500 m, (modified from Brunet et al., 2017). Coring site U1401 is located on Deposit 3 and consists of a 900 m transect with four holes (C, A, B, D from East to West); **c**) Detail of the west flank of Montagne Pelée volcano marked by horseshoe shaped structures deriving from flank collapses. First flank-collapse structure is labeled in red, the second in green and the third in yellow (from Le Friant et al, 2003).

Figure 2. a) Photo of the first section (1H) of the core U1401A. Hemipelagic mud (brown squares, H) appears in clear beige color; turbidites (yellow squares, T1 to T5) are more characterized by a dark brown color and significant thickness. Tephra layers (orange lines, t) have features similar to turbidites and low thickness; this makes it difficult to simply recognize them to the naked eye. A more detailed description of tephra layers has been done by counting operation; **b**) Synthetic log of the whole core U1401A. In brown: turbidites (T1 to T10); in beige: hemipelagic mud; in orange: tephra layers (t). Abundance of volcanic fragments in each tephra layer and in volcanoclastic turbiditic deposits obtained from counting operations: in green scoria, in red pumices and in blue lava dome clasts; Six peaks of pumices can be recognized along the core, four in the first 300 cm and two others in the deep part of the core at depth of 700 and 800 m. Two peaks of scoria are found at about 700 m. Lava dome clasts prevail all along the core with percentages rarely going lower than 20%; **c)** Isotopic $\delta^{18}O$ and ^{14}C results on core U1401A: in blue $\delta^{18}O$ results, In red: ^{14}C dating for the three marker points at 197, 348.5 and 488.5 cm in the core). $\delta^{18}O$ values exhibit variations from -2,52 to 0,07 ‰, with high values in the deep part of the hole and isotopic maximum recorded at about 650 cm in depth.

885 **Figure 3. a**) Correlation between GRA density and magnetic susceptibility data along the
886 core U1401A; on the right side simplified log of the core: in brown turbiditic
887 deposits (T1 to T10), in grey scoria layers and in beige sections parts of the core
888 with prevalence of hemipelagic mud (Hem.); **b**) Detail of magnetic susceptibility
889 data for the section 1H2 of the core. Six tephra layers, one turbiditic deposit and six
890 hemipelagic mud can be recognized in the section following the positive and
891 negative peaks in data.

892

893 **Figure 4.** SEM images of three representative volcanic fragments with a magnification of x35
894 and x75 for the top images and x300 for the more detailed lower images. **a**) Lava
895 dome clasts: characterized by low vesicularity and highly microcristallized matrix
896 glass; **b**) Pumice clasts: usually well vesiculated, characterized by large matrix
897 glass and no microlite; **c**) Scoria clasts: with well-developed thicker matrix glass,
898 partially microcristallized.

899

900 **Figure 5. a)** Evolution of the SiO_2 content of volcanic clasts (matrix glasses) along depth in
901 the core U1401A. Single point measurements on matrix glass of different glass
902 shards are represented. Pumice clasts (red circle) present one main compositional
903 range b between 70 and 79 wt% SiO_2, whilst scoria clasts (green circle) exhibit
904 amore basic compositional range, between 64 and 70 wt% SiO_2 . Within the scoria-
905 rich levels, some more silicic clasts of similar composition as the pumice clasts are
906 present (light red diamonds).; **b)** K_2O vs. SiO_2 diagram of matrix glass of the glass
907 shards of the core U U1401 and little matrix glass from U 1401B, C and D. The
908 domains of residual glass from on-land deposits are also reported: pumices (blue)

and scoria clasts (purple) from Montagne Pelée (Boudon et al., 2013) and pumices from the neighboring island of Dominica (orange) (Balcone-Boissard et al., 2018).

Figure 6: a) Modeled age of the core U 1401 A and correlation with the core CAR-MAR 4 (Boudon et al., 2013). The curve in calibrated age for the core U14101A is issued from the correlation with the core CAR-MAR 4. The final modeled age returns a bottom core age of 36425 cal yr BP and a mean sedimentation rate of ~22 cm/ka coherent with the values known for the basin. The model returns some important gaps of ~6 ky in the sedimentary record due to the erosive power of turbidites; **b)** Comparison of tephra records in between the core U1401A (top) and the core CAR-MAR 4 (bottom). In U1401A red lines: pumice tephra; green lines: scoria tephra; blue lines: lava dome clast tephra; brown rectangles: turbiditic deposits. In CAR-MAR 4 all red lines indicate tephra levels in the core. The tephra records in between the two cores is consistent, with the same change in tephra typology from scoria clasts in the bottom of the cores to lava dome and pumice clasts at the top of the cores.

Figure 7: Ages of tephra layers depending on the depth in the core. In red pumice layers, in green scoria layers and in blue lava dome clast layers. Finally 24 tephra layers are recognized with: alternating of pumice and lava dome clasts in the first 10 cal. ka BP, prevalence of dome-forming eruptions in the period 13-16 cal. ka BP and finally explosive scoria eruption, plinian eruption and dome-forming eruption in the period 25-30 cal. ka BP.

Figure 8 : The recent volcanic history of Montagne Pelée: toward a new model of evolution. Comparison with previous works.

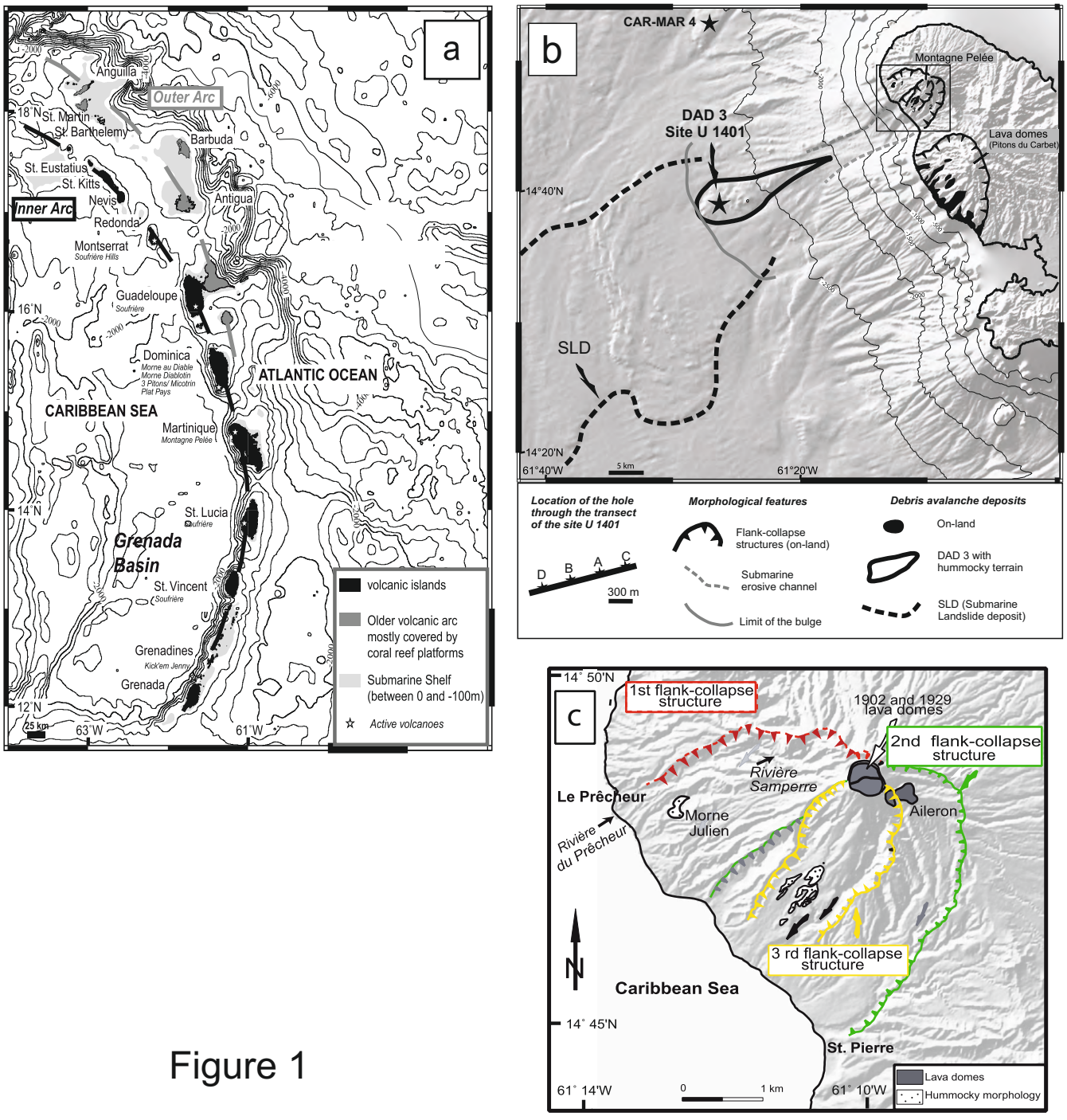
a
Anguilla
Outer Arc
18°N
St. Martin
St. Barthelemy
Barbuda
St. Eustatius
St. Kitts
Nevis
Antigua
Inner Arc
Redonda
Montserrat
Soufrière Hills
Guadeloupe
Soufrière
16°N
Dominica
Morne au Diable
Morne Diablotin
3 Pitons/ Micotrin
Plat Pays
ATLANTIC OCEAN
CARIBBEAN SEA
Martinique
Montagne Pelée
14°N
St. Lucia
Soufrière
Grenada Basin
St. Vincent
Soufrière
Grenadines
Kick'em Jenny
Grenada
12°N
25 km
63°W
61°W
volcanic islands
Older volcanic arc mostly covered by coral reef platforms
Submarine Shelf (between 0 and -100m)
Active volcanoes
b
CAR-MAR 4
Montagne Pelée
DAD 3
Site U 1401
Lava domes
(Pitons du Carbet)
14°40'N
SLD
14°20'N
61°40'W
5 km
61°20'W
Location of the hole through the transect of the site U 1401
D
B
A
C
300 m
Morphological features
Flank-collapse structures (on-land)
Submarine erosive channel
Limit of the bulge
Debris avalanche deposits
On-land
DAD 3 with hummocky terrain
SLD (Submarine Landslide deposit)
c
14° 50'N
1st flank-collapse structure
1902 and 1929 lava domes
2nd flank-collapse structure
Rivière Samperre
Le Prêcheur
Morne Julien
Aileron
Rivière du Prêcheur
N
3 rd flank-collapse structure
Caribbean Sea
14° 45'N
St. Pierre
61° 14'W
0
1 km
61° 10'W
Lava domes
Hummocky morphology

Figure 1

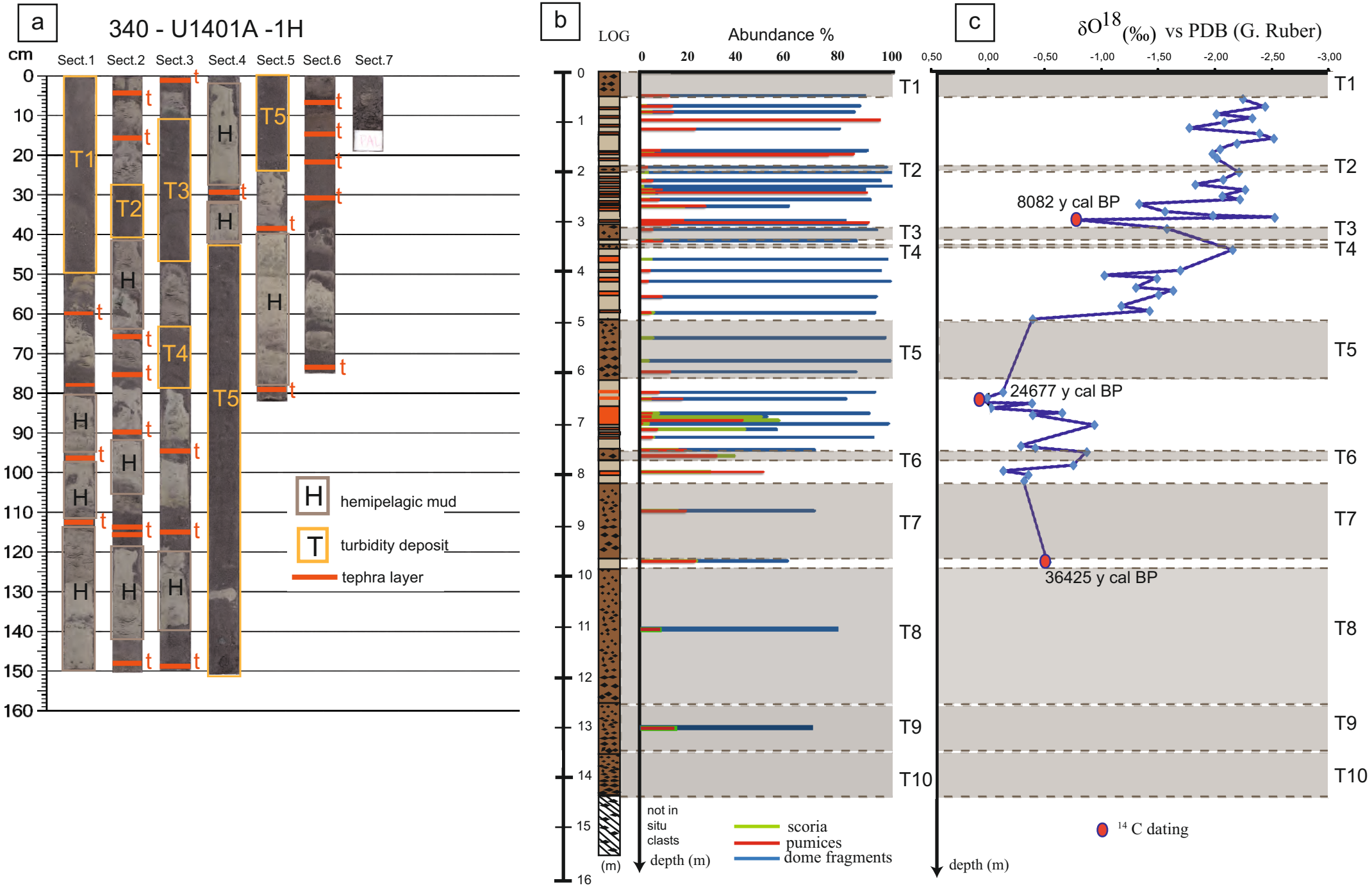
a
340 - U1401A -1H
cm
Sect.1
Sect.2
Sect.3
Sect.4
Sect.5
Sect.6
Sect.7
T1
T2
T3
T4
T5
H
t
hemipelagic mud
turbidity deposit
tephra layer
b
LOG
Abundance %
not in situ clasts
scoria
pumices
dome fragments
depth (m)
c
δO18 (‰) vs PDB (G. Ruber)
8082 y cal BP
24677 y cal BP
36425 y cal BP
14 C dating
depth (m)

Figure 2

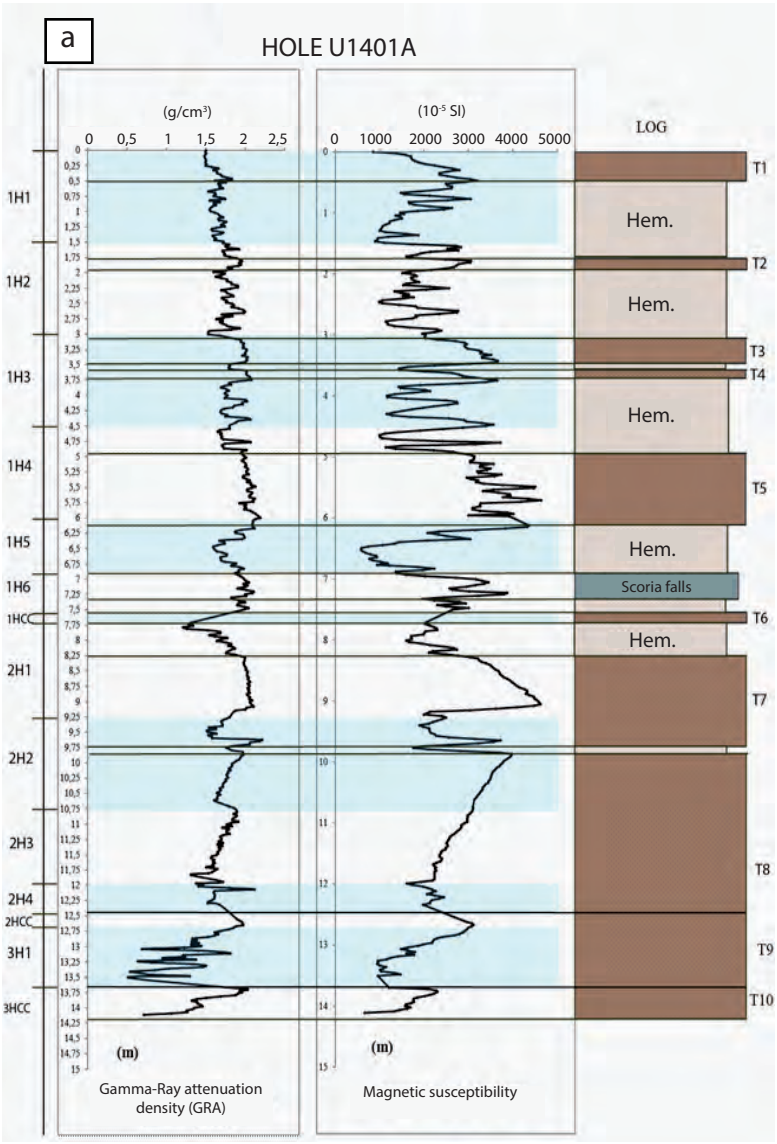
a
HOLE U1401A
(g/cm³)
0 0,5 1 1,5 2 2,5
(10⁻⁵ SI)
0 1000 2000 3000 4000 5000
LOG
1H1
1H2
1H3
1H4
1H5
1H6
1HCC
2H1
2H2
2H3
2H4
2HCC
3H1
3HCC
T1
T2
T3
T4
T5
T6
T7
T8
T9
T10
Hem.
Hem.
Hem.
Hem.
Scoria falls
Hem.
(m)
(m)
Gamma-Ray attenuation density (GRA)
Magnetic susceptibility

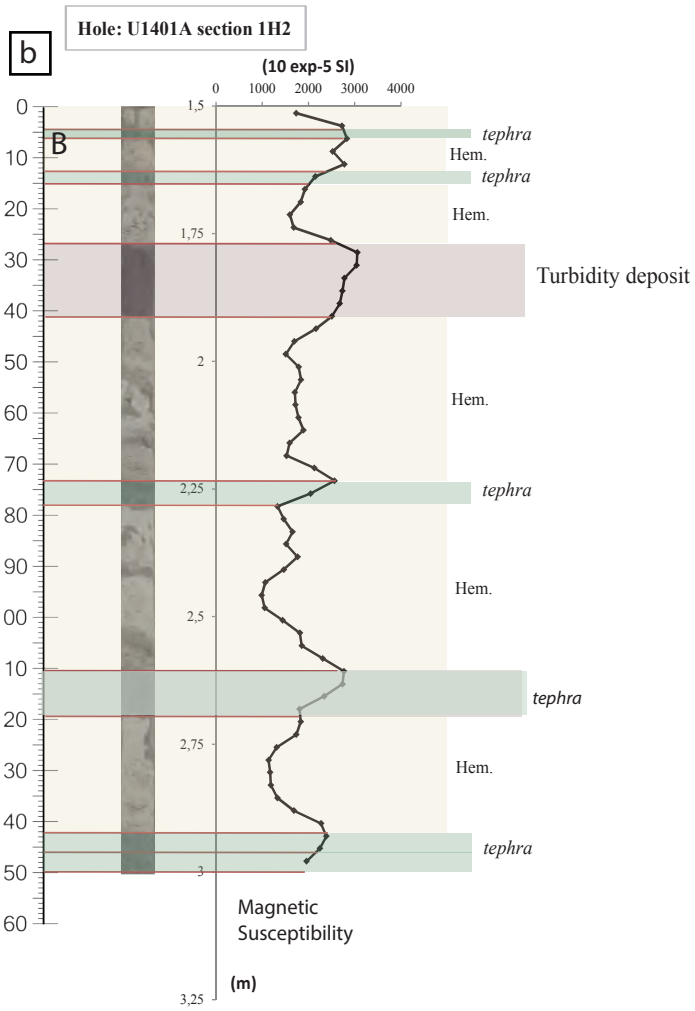
b
Hole: U1401A section 1H2
(10 exp-5 SI)
0 1000 2000 3000 4000
B
tephra
Hem.
tephra
Hem.
Turbidity deposit
Hem.
tephra
Hem.
tephra
Hem.
tephra
Magnetic Susceptibility
(m)

Figure 3

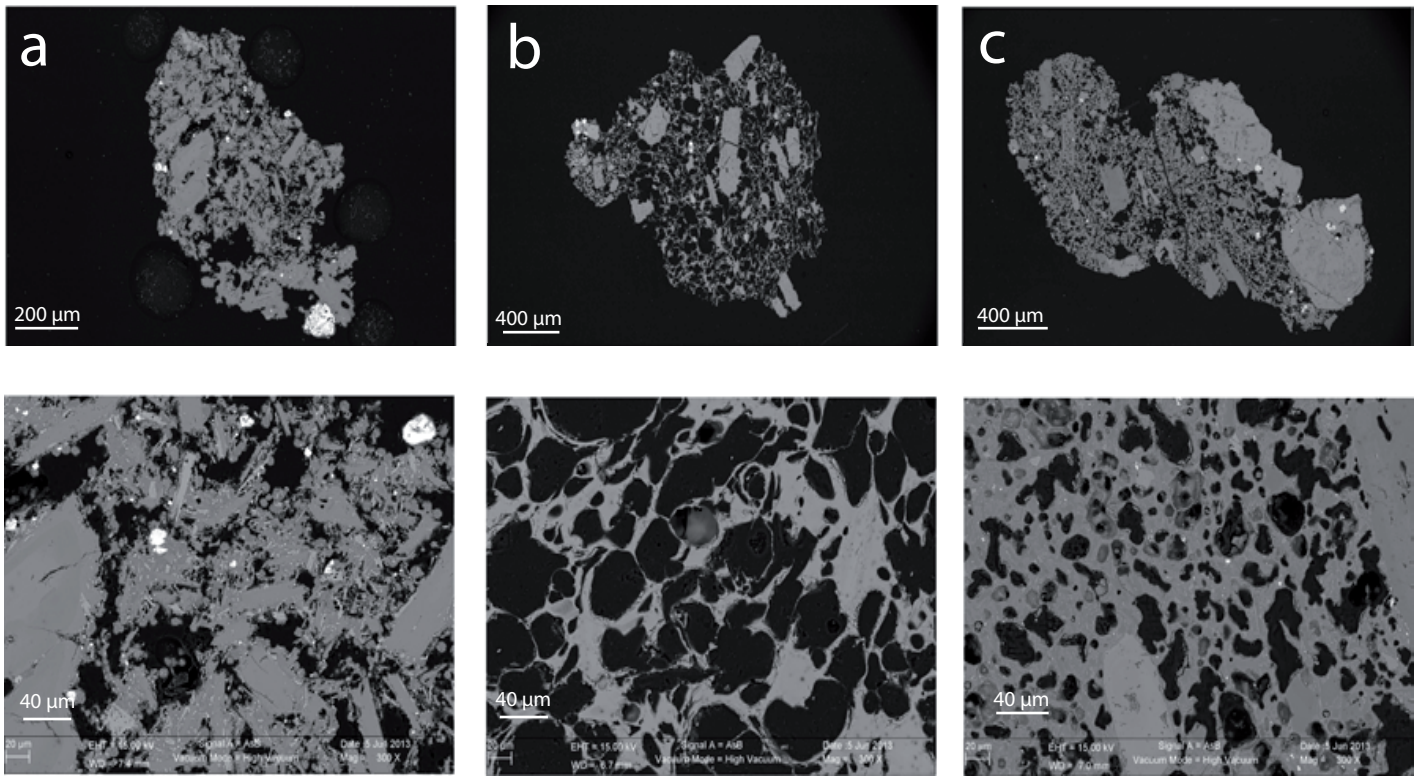

Figure 4

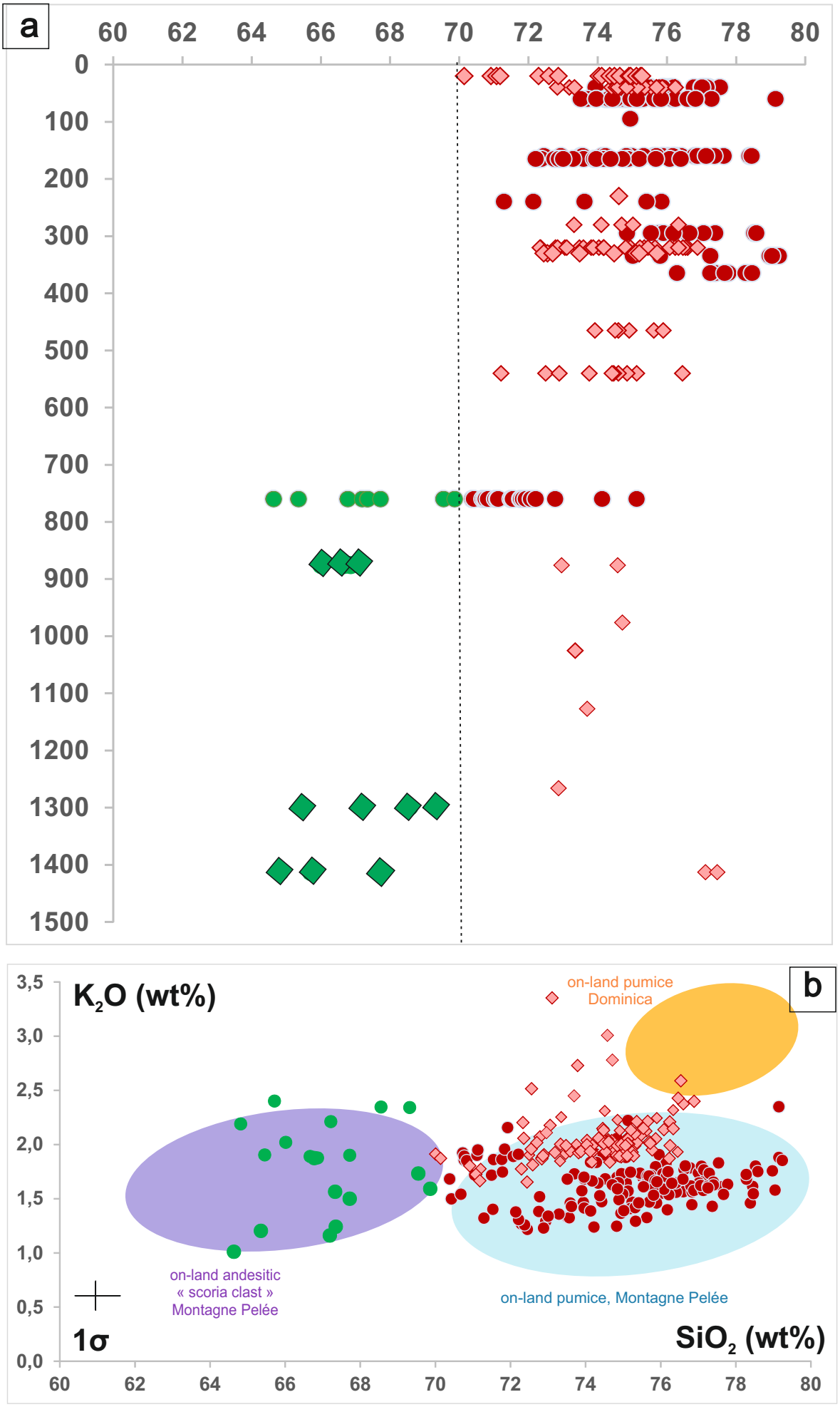

scoria

tephra

turbidite

Figure 5

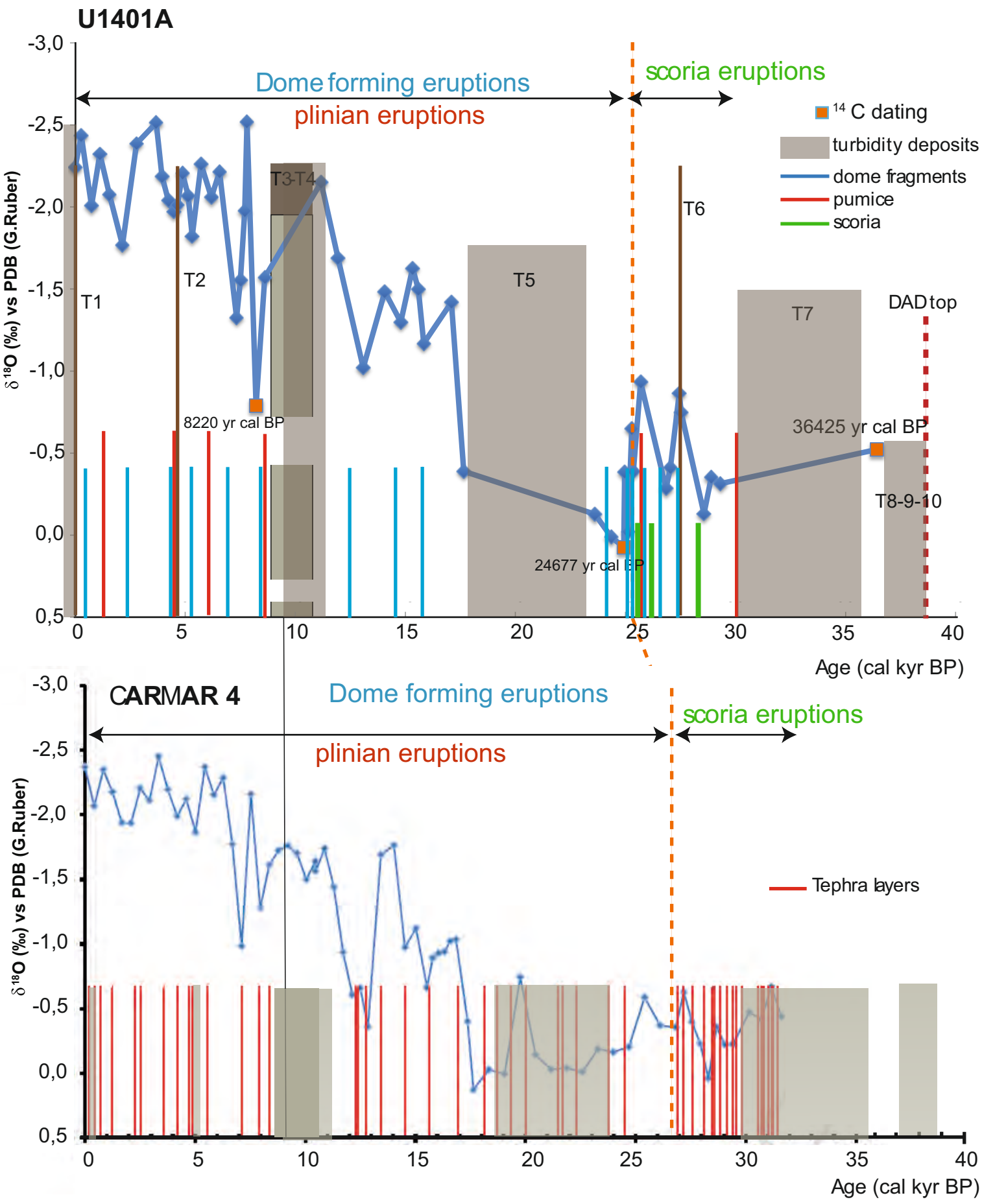
U1401A
Dome forming eruptions
plinian eruptions
scoria eruptions
14 C dating
turbidity deposits
dome fragments
pumice
scoria
T1
T2
T3-T4
T5
T6
T7
T8-9-10
DAD top
8220 yr cal BP
24677 yr cal BP
36425 yr cal BP
δ18O (‰) vs PDB (G.Ruber)
Age (cal kyr BP)
CARMAR 4
Dome forming eruptions
plinian eruptions
scoria eruptions
Tephra layers
δ18O (‰) vs PDB (G.Ruber)
Age (cal kyr BP)

Figure 6

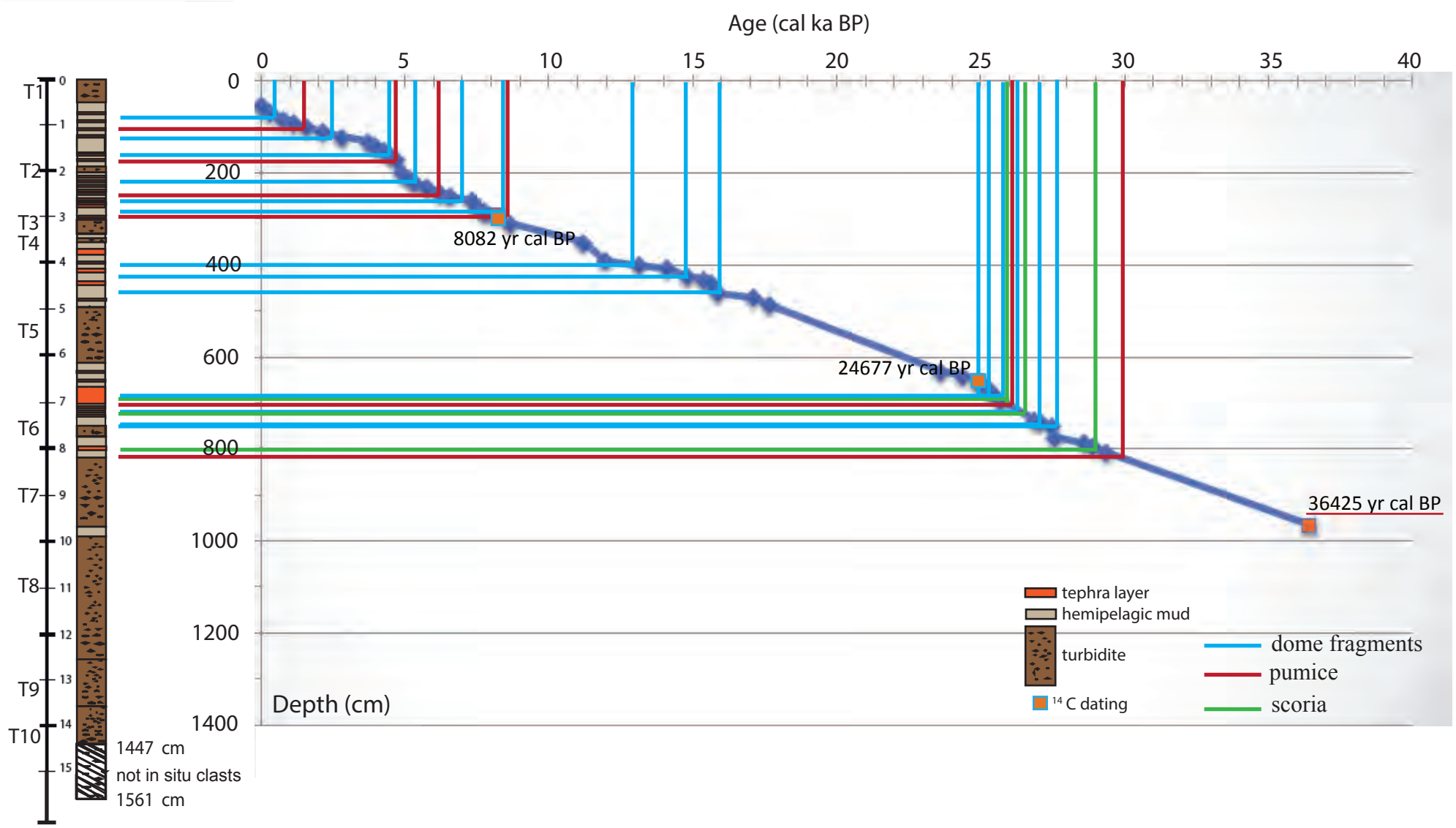
Age (cal ka BP)
0
5
10
15
20
25
30
35
40
0
200
400
600
800
1000
1200
1400
Depth (cm)
8082 yr cal BP
24677 yr cal BP
36425 yr cal BP
T1
T2
T3
T4
T5
T6
T7
T8
T9
T10
1447 cm
not in situ clasts
1561 cm
tephra layer
hemipelagic mud
turbidite
14 C dating
dome fragments
pumice
scoria

Figure 7

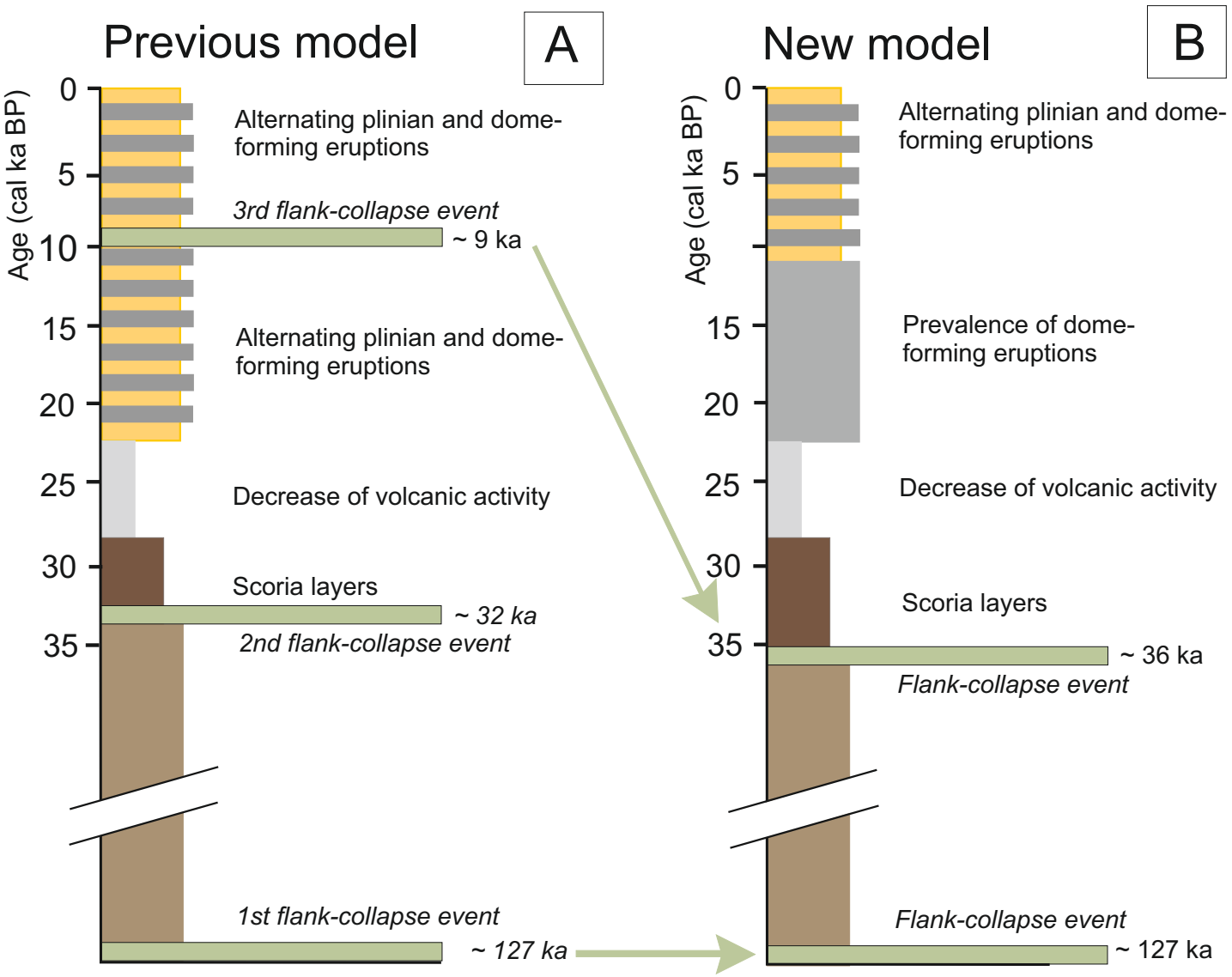
Previous model
A
New model
B
Age (cal ka BP)
0
5
10
15
20
25
30
35
Alternating plinian and dome-forming eruptions
3rd flank-collapse event
~ 9 ka
Alternating plinian and dome-forming eruptions
Decrease of volcanic activity
Scoria layers
~ 32 ka
2nd flank-collapse event
1st flank-collapse event
~ 127 ka
Alternating plinian and dome-forming eruptions
Prevalence of dome-forming eruptions
Decrease of volcanic activity
Scoria layers
~ 36 ka
Flank-collapse event
Flank-collapse event
~ 127 ka

Figure 8